American Journal of Geophysics, Geochemistry and Geosystems
Vol. 7, No. 3, 2021, pp. 110-125
http://www.aiscience.org/journal/aj3g
ISSN: 2381-7143 (Print); ISSN: 2381-7151 (Online)

Geomorphological Analysis of Taj Mahal Area Using Remote Sensing and GIS

Kuldeep Pareta[1, *], Upasana Pareta[2]

[1]DHI (India) Water & Environment Pvt Ltd., New Delhi, India
[2]Omaksh Consulting Pvt Ltd., Greater Noida, UP, India

Abstract

Space-borne and airborne technology has comprehensively used in geomorphology since longer than a century because these technologies are benefited with landform analysis, geomorphic feature extraction, and improvements in mapping techniques. It has been extensively used in geomorphology since 1972, when Landsat series data (from 1972 to present) are freely available, and it has also fulfilled the analytical requirements of geomorphologists. In this study L-band ALOS/PALSAR, Sentinel-1, C-band SRTM, Landsat-8 OLI have been used to assess the geological structures, and geomorphological investigation/mapping of the study area (within 25 Km buffer from the center of Taj Mahal), while Landsat series data from 1972 to 2021 at 5 years interval have been applied for river morphology and urban geomorphology analysis. Geomorphologically, the area has been classified as upland/older alluvial plain-Varanasi older alluvial plain (VOAP), and low land older flood plain including erosional terrace, depositional terrace active flood plain of present-day rivers. Geo-strata of the area around Taj Mahal were found as clay (RL 149-133 m), non-plastic to silty-sand (RL 133-123.8 m), thicker clay layer (RL 123.8-60.3 m), and fine-to-medium-grained quarzitic sandstone (below then 60.3 m). The mean river width (1972-2021) of Yamuna River right behind the Taj Mahal is 149.6 m, while average sinuosity index of the study reach is 2.31 which corresponding to the highly meandering form of the river, because tectonic control is less powerful than other variables, the meandering is more influenced by the gradient, lithology and river surrounding. meander bends migration rate has been observed at d/s of Taj Mahal, as two spurs, u/s of Taj Mahal have been installed to train the river and avoid any danger to the structure of Taj Mahal. Through the cross-sectional profile analysis, some human intervention has observed behind the Taj Mahal, and notices that a low-level weir up to a RL of 146 m has been constructed across the Yamuna River to create a permanent lake of water behind the Taj Mahal. Agra city has experienced a significant urban growth in the last 50 years (1972-2021), it has increased 1284% of urban area with an average growth rate of 2.88 Km^2 per year, while population has increased only 282%. Till 2001 urban area is limited to only one geomorphic unit of older alluvial plain, but onwards due to Immanent of population increment it has been extended to other geomorphic units which are not good for the residence purpose.

Keywords

Geomorphology, Geo-strata, River Morphology, Urban Expansion, Taj Mahal, RS/GIS

Received: July 2, 2021 / Accepted: August 11, 2021 / Published online: August 23, 2021

1. Introduction

Geomorphology is deal with the origin of relief forms of the surface of the earth's crust, including several of the natural processes that are responsible for the forms of the Earth's surface. Understanding the environment in which we live requires an understanding of the various processes that lead to landforms. A geomorphological map of an area should give information about the morphology (appearance), morpho-

* Corresponding author
E-mail address: kpareta13@gmail.com (K. Pareta), kupa@dhigroup.com (K. Pareta)

metry (dimension / slope), morphogen (origin) and morpho-chronology (the age) of each form [1]. Understanding various earth surface processes, landscape evolution, geochronology, structural characteristics, natural resource inventory and mapping, and natural hazards requires geomorphological mapping and analysis of various processes in fluvial environments, while remote sensing can provide information on the location / distribution of landforms, surface/sub-surface composition, and natural hazards [2]. Earth observations from space utilising optical, thermal, and radar remote sensing instruments have aided in the resolution of significant geomorphological and geological problems on a variety of scales [3].

Advances in remote sensing methodology have constantly benefited geomorphology by improving mapping technology, form analysis, and feature discrimination [2]. Space-borne and airborne technology now not a new technology, it has been widely used since over a century. The aerial perspective was an integral part of the physiographic analysis [4-7].

Beginning in the 1930s, government agencies in the United States enlisted the help of various resource experts, including foresters, pedologists, hydrologists, and civil engineers, to undertake resource inventories using landform interpretation methodologies. In Europe, the work of [8-9] demonstrated the growing importance of aerial photography in academic geomorphology. The work of [10-13] demonstrated to the engineering and earth scientific communities that these techniques were more than just mapping tools, and that they could be used as data resources and field tools. The work of [10-13] demonstrated to the engineering and earth scientific communities that these techniques were more than just mapping tools, and that they could be used as data resources and field tools. The use of thermal infrared scanners by [14], imaging radar by [15], and space platforms by [16] opened the path for today's remote sensing applications in geomorphology. Satellite remote sensing imagery has been widely used in geomorphology since 1972, when Landsat series data (from 1972 to present) became freely available, and because of its worth, which can be measured by how well it meets geomorphologists' investigative needs [17].

Geomorphic features have been successfully identified using space-based radar sensors [18-20]. Because microwave EM radiation can probe near-surface features [21] and may be utilised to investigate active and inactive geological formations and geomorphological features using distinct time-series satellite photos, this research has been conceivable [22]. Surface changes and spatiotemporal dynamics have also benefited from the interferometric SAR (InSAR) coherence approach [22-25]. Remote sensing, as opposed to traditional in situ measurements, has allowed for continuous monitoring of the Earth's surface at varied spectral, spatial, and temporal resolutions [26-27]. Remote sensing data including GIS, digital elevation model (DEM) data, digital surface model (DSM) data, GPS/DGPS, LiDAR data, Radar data, and drone-based sensor imagery have enhanced the capability to understand the surface processes more clearly and improve the accuracy in geomorphological mapping. Authors also conducted several studies on geomorphology investigation and mapping using satellite remote sensing data and GIS [28-45].

In this study, space-borne remotely sensed imagery of various types of viz. L-band Advanced Land Observing Satellite (ALOS) / Phased Array Type L-band Synthetic Aperture Radar (PALSAR), C-band Shuttle Radar Topography Mission (SRTM), Sentinel-1, Landsat-8 Operational Land Imager (OLI) and Google Earth have been used in a complementary manner to assess the geological structures, geomorphological investigation and mapping of the study area. Landsat-1 MSS, Landsat-2 MSS, Landsat-3 MSS, Landsat-5 TM, Landsat-7 ETM+, and Landsat-8 OLI have been used for river morphology (mean river width, sinuosity index, and meander bends trend analysis) and urban expansion / urban geomorphology analysis.

2. About the Study Area

The Taj Mahal was built between 1631 and 1648 on the right bank of the Yamuna River in Agra, Uttar Pradesh, at 27° 10' 30.44" N latitude and 78° 02' 31.25" E longitude, more than 373 years ago. The Taj Mahal's major component is the tomb, which is composed of white marble and has a height of 73 metres above ground level. It's a gigantic edifice weighing in at over 12,000 tonnes [46].

The study area has been selected 25 Km buffer from the center of Taj Mahal. Within this area, geology, geomorphology, urban geomorphology, and subsoil investigation has been done. A 114 Km long river reach of the Yamuna River (which is fall within the buffer area) is also selected for river morphology study i.e. mean river width, and sinuosity index. Yamuna river is a meandering river, and Taj Mahal is located on a meander bend, therefore, authors have decided to do the meander bends trend of the study area. For meander bend trend analysis total 12 bends have selected in study reach of Yamuna River (Figure 1).

The study area situated in the extreme south-west corner of the Uttar Pradesh state. It is a part of the southern upper Ganga plain. Based on geology, soils, topography climate and natural vegetation, the study area can be divided into two physiographic division: (a) Yamuna Khadar, and (b) Agra Plain. Yamuna Khadar is situated parallel to river Yamuna with an average width of 10 Km to 15 Km. The slope is according to the direction of flow of river Yamuna, meanders

and ravines are the main topographic feature in this division. Agra Plain is a flat plain sloping towards south-east direction.

The climate of the study area is characterized by extremely hot summers, a cold winter and general dryness throughout the year except the southwest monsoon. The winter season in Dec-Feb is followed by the summer season which continues till mid-June and is followed by the monsoon season which continues till the end of Sep. The maximum temperature during hot touches has reached 45°C while during winters it comes to 5°C. The average annual rainfall of the study area is 695 mm. Four National Highways (NH) have passed through the study area. These are: NH-44 route from New Delhi to Gwalior, NH-19 route from Agra to Kanpur, NH-21 route from Jaipur to Bareilly, NH-509 route from Agra to Moradabad. The study area is also well connected to major cities of India by Indian railways and airlines.

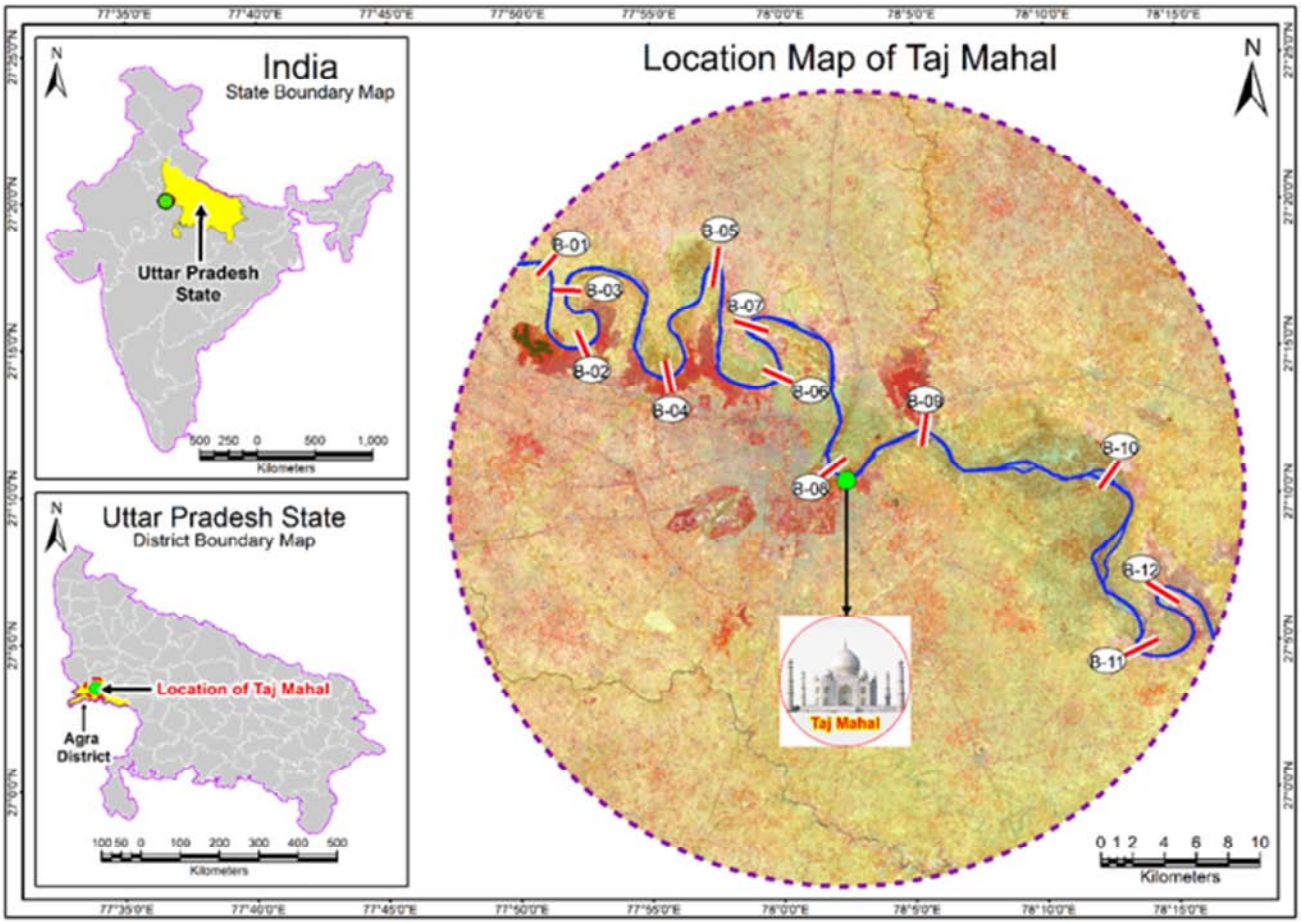

Figure 1. Location Map of Taj Mahal, Agar (Uttar Pradesh).

3. Data Used and Their Sources

Landsat series satellite data from 1972 to 2021 (at 5 years interval, 11 datasets in total) have been downloaded from Earth Explorer, USGS: https://earthexplorer.usgs.gov. The spatial resolution of these datasets is ranging between 57*79 m and 30 m.

The DEM data for the Shuttle Radar Topography Mission (SRTM) were gathered from the United States Geological Survey (USGS) in partnership with NASA and the National Geospatial-Intelligence Agency (NGA): https://earthexplorer.usgs.gov. Using a single microwave C-band X-SAR-SRTM with 30 m spatial resolution, several sceneries were analysed and combined into a mosaic to gain comprehensive topographic information.

The Sentinel-1 Synthetic Aperture Radar (SAR)-IW satellite imagery with 5*20 m spatial resolution of year 2021 has been download from Alaska Satellite Facility (ASF): https://search.asf.alaska.edu/#/. The detail of these datasets with acquisition date, satellite name, sensor type, and spatial resolution is given in Table 1.

Table 1. Type of Satellite Remote Sensing Data.

S. No.	Acquisition Date	Satellite Name	Sensor Type	Spatial Resolution (m)
1	14th November 1972	Landsat-1	MSS	57*79
2	26th March 1977	Landsat-2	MSS	57*79
3	10th September 1981	Landsat-3	MSS	57*79
4	11th January 1986	Landsat-5	TM	30
5	14th March 1991	Landsat-5	TM	30
6	09th March 1995	Landsat-5	TM	30
7	05th February 2001	Landsat-5	TM	30
8	31st March 2006	Landsat-7	ETM+	30
9	06th April 2011	Landsat-5	TM	30
10	21st May 2016	Landsat-8	OLI	30
11	01st April 2021	Landsat-8	OLI	30
12	18th May 2021	Sentinel-1A	IW	5*20
13	23rd September 2014	SRTM	X-SAR	30

MSS = Multispectral Scanner, TM = Thematic Mapper, ETM+ = Enhanced Thematic Mapper Plus, OLI = Operational Land Imager, IW = Interferometric Wide swath, SRTM = Shuttle Radar Topography Mission, SAR = Synthetic Aperture Radar.

Apart from above stated datasets, geological maps have been collected from Geological Survey of India (GSI): http://www.portal.gsi.gov.in.

Subsoil data has been accumulated from published article which were conducted by [47-52], as well as some literature has been collected from Archaeological Survey of India (ASI): https://asi.nic.in/?s=tajmahal.

Agra city population data has been collected from Census of India website: https://censusindia.gov.in for year 1971, 1981, 1991, 2001, and 2011; while the projected population data of year 1977, 1986, 1995, 2006, 2016, and 2021 has been collected from United Nations World Population Prospects (https://www.macrotrends.net/cities/21151/agra/population).

4. Methodology

The remote sensing and GIS methods and other statistical data techniques have been comprehensively used for geological, subsoil investigation, geomorphological, river morphology, and urban geomorphological analysis of the area around Taj Mahal. This study looked at Landsat satellite images of the predominantly dry season (Mar-Apr-May) from 1972 to 2021 (11 total). The satellite imageries were shot during the dry season to avoid overestimation of the river's expanse, which is frequent with images taken during high flow or monsoon and flooding seasons. There were no clouds in the satellite image data that was chosen.

The Landsat satellite images from 1972 to 2021 have been download from Earth Explorer, USGS. These raw data or separate bands have been stored in a specific folder and by using ArcGIS 10.7.1 software (with ArcToolbox => Data Management Tools => Raster => Raster Processing => Composite Bands) these satellite imageries have been geo-processed including the removal of haze and noise. Agra city and surrounding area is fall in two UTM zones (43, and 44), but major part of the study area fall in UTM zone no 43, so it has decided the projection system - Universal Transverse Mercator (UTM) zone no. 43, and datum - the World Geodetic System 1984 (WGS-84) was employed, for better calculation and verification of distances between utilities, banklines, river infrastructure, span length, and urban expansion, the World Geodetic System 1984 (WGS-84) was employed. An automatic produced Root Mean Square Error (RMSE) of less than 0.23 has been maintained. Various digital image processing and visual image interpretation techniques have used for geological and geomorphological mapping of Taj Mahal, as well as river morphology and urban expansion study.

5. Result and Discussion

5.1. Geology

A general lithological map can help understanding of the geomorphology of an area. Published geological quadrangle maps of 54-E and 54-I (which is fall in Agra city) have been downloaded from Geological Survey of India (GSI) website: http://www.portal.gsi.gov.in. These maps have been geo-referenced and digitized and prepared a geological map of Taj Mahal. This geological map has been updated through Landsat-8 OLI satellite imagery (30 m spatial resolution), SRTM DEM data (30 m spatial resolution) with slope map, landform map, and Survey of India (SoI) topographical maps (1:50,000 scale) with limited field check. A geological map of Taj Mahal is shown in Figure 2.

Various geologists have contributed to the study area's various geological characteristics. Among them are [33, 53-64], others, and so forth. They have recorded the principal rock formations as described in Table 2.

Table 2. Lithostratigraphic Succession of Taj Mahal.

Map Symbol	Geological Unit	Lithology	Group	Age	
Q_2fc	Channel Alluvium	Grey, fine to medium grained cross bedded to laminated, micaceous sand with capping of overbank silt. (Active Flood Plain)	Newer Alluvium	Holocene	Quaternary
Q_2ft	Terrace Alluvium	Cyclic sequence of grey, fine to medium grained, micaceous sand and laminated grey silt-clay. (Older Flood Plain: Depositional Terrace - T1, T1a)			
Q_1fo	Varanasi Alluvium	Polycyclic sequence of oxidized Khaki silt-clay with or without kankar and yellowish brown, fine to medium, micaceous sand. Q_1fo_c: Silt-clay facies, Q_1fo_s: Sandy facies. (Varanasi Older Alluvial Plain and Erosional Terrace of Older Flood Plain - Te)	Older Alluvium	Middle to Upper Pleistocene	

Source: Geological Survey of India (GSI)

The area is largely covered by a thick layer of Quaternary sediments classified as (i) Older Alluvium and (ii) Newer Alluvium geologically. Varanasi Alluvium, which is from the Middle to Late Pleistocene age, represents the Older Alluvium. Newer Alluvium of Holocene age comprises two units viz. (i) Terrace Alluvium and (ii) Channel Alluvium.

Varanasi Older Alluvium is an extensively developed polycyclic, sequence of yellowish khaki silty clay with kankar and ferruginous concretions and brown to grey colour micaceous sand. Surficially, the sediments have been classified into widely developed silt-clay facies and sandy facies. Silt-clay facies comprises oxidized khaki to brownish colors silt-clay with disseminated kankar nodules. At places calcrete horizon, enclosing lenses of honeycomb type of kankar, is present which comprises several gastropod shells like, Lymnea sp. And Planorbis sp. The sandy facies represent scattered sand mounds and sandy flats and is made up of oxidized light brown to deep khaki. In exposed sections sand bed comprises brown to reddish brown and grey micaceous sand exhibiting horizontal laminations, ripple marks and worm burrows (Skolithos).

The Terrace Alluvium is restricted in the valley zones of Yamuna within their depositional domain. In Yamuna single depositional terrace represents Terrace Alluvium. It is mainly composed of alternate sequence of silty clay and fine to medium grained, micaceous sand, mainly of grey colors replete with sedimentary structures like parallel laminations, cross bedding, ripple marks etc. The sand comprises 75 to 80% of quartz whereas remaining 25 to 20% comprises mica, opaques, and rock fragments.

The Channel Alluvium of Yamuna River is represented by fine to medium grained, light grey, micaceous, cross bedded to laminated sand of point bars, channel bars, and lateral bars with occasional overbank silt capping at places.

The area is poor in mineral resource. Reh (alkaline soil) is found at places over Varanasi Alluvium, which is utilized locally as washing detergent. Clay, occurring extensively on Varanasi Alluvium, is used for local pottery production and brick making. Sand Occurring in riverbed is widely used in masonry work.

5.2. Geomorphology

Remote sensing data is an important resource for interpretation and preparation of geomorphological map. A detailed geomorphological map of the Taj Mahal has been prepared by using visual image interpretation of Sentinel-1 Synthetic Aperture Radar (SAR)-IW satellite imagery with 5x20 m spatial resolution, Landsat-8 OLI satellite imagery with 30 m spatial resolution, SRTM DEM data with 30 m spatial resolution, geological quadrangle maps with structural and lithological maps from Geological Survey of India (GSI) (1: 250,000 scale), and Survey of India (SoI) topographical maps (1: 50,000 scale) with limited field check, and shown in Figure 2. The various geomorphic units and their components have identified and mapped. Important geomorphic units of the Taj Mahal area are given in Table 3.

Table 3. Important Geomorphic Units of the Taj Mahal.

S. No.	Geomorphic Origins	Geomorphic Landforms	Geomorphic Primary Units	Geomorphic Secondary Units
1	Fluvial Origin	Flood Plain	Active Flood Plain	Active Flood plain
2	Fluvial Origin	Flood Plain	Active Flood Plain	Channel Bar
3	Fluvial Origin	Flood Plain	Active Flood Plain	Lateral Bar
4	Fluvial Origin	Flood Plain	Active Flood Plain	Point Bar
5	Fluvial Origin	Flood Plain	Active Flood Plain	Abandoned Channel
6	Fluvial Origin	Alluvial Plain	Older Alluvial Plain	Older Alluvial Plain
7	Fluvial Origin	Alluvial Plain	Older Alluvial Plain	Gullied Tract
8	Fluvial Origin	Alluvial Plain	Older Alluvial Plain	Oxbow Lake
9	Fluvial Origin	Flood Plain	Older Flood Plain	Older Flood plain
10	Fluvial Origin	Flood Plain	Older Flood Plain	Meander scar
11	Fluvial Origin	Flood Plain	Older Flood Plain	Abandoned Channel
12	Water Bodies	Water Bodies	Ponds, Lakes	Ponds, Lakes
13	Water Bodies	Water Bodies	River	River

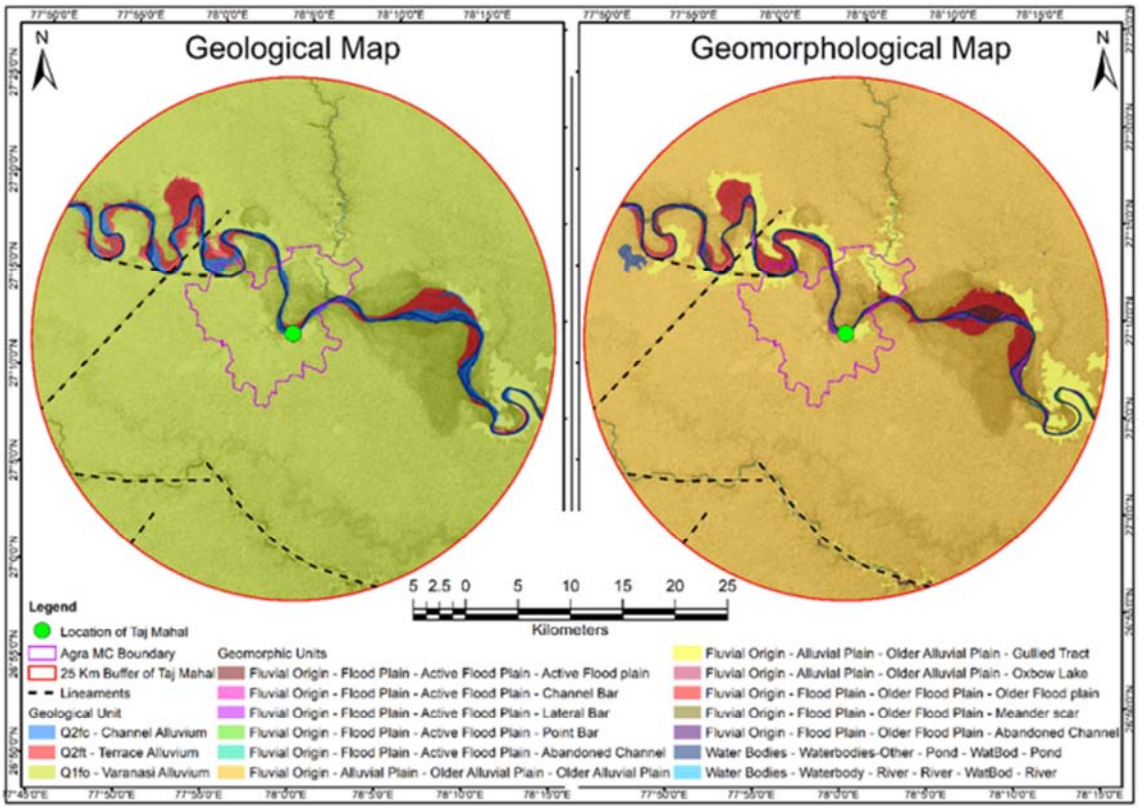

Figure 2. Geological and Geomorphological Map of the Study Area.

The area has been classified into two broad geomorphic units viz. an Upland or Older Alluvial Plain termed as Varanasi Older Alluvial Plain (VOAP), and a Low Land or Flood Plain comprising Older Flood Plain, divisible into Erosional Terrace (Te) and Depositional Terrace (T1, T1a), and Active Flood Plain of present-day rivers. The most developed Varanasi Plain is the oldest geomorphic surface free form floods, representing a flat terrain without any marked relief variations. It demarcates its boundary with the flood plain by a well-defined scarp. It has a general south-easterly slope. It is dotted by few tals. Badland is developed along Yamuna River.

The Varanasi Older Alluvial Plain, the height and the oldest geomorphic unit covering maximum part of the area, ranges in elevation from 152 m to 188 m above msl with a general south-easterly master slope. It is a flat alluvial terrain with relief variations at micro-level. This plain has been classified into two surfaces viz. a flat silt-clay surface and a humpy sandy surface. The latter comprises sandy flat, mounds and ridges. The height of sandy mounds and ridges extends up to 6 m above ground level. A very wide zone, trending NW-SE comprising greater concentration of tals and palaeo-channels as well as patches infested by soil sodacity or reh passes through the area. The water table is also shallow in this zone. This zone represents an older phase of active channel.

The Older Flood Plain of river Yamuna comprises a single depositional terrace on either bank. It is separated from the VOAP by a scarp 3 m to 5 m high. The higher terrace (T1) ranging in elevation from 168 m to 173 m above msl is a more-or-less flat surface with several abandoned channels. The lower Terrace (T1a) is slightly undulatory and restricted as narrow lenticular patched along the river course. Its elevation ranges from 157 m to 164 m above msl. It is separated from T1 terrace by a gradual and undistinctive scarp about 1 m to 1.5 m high.

The Older Flood Plain of Yamuna River is represented by two terraces i.e. a Higher Erosional Terrace (Te), and a Lower Depositional Terrace (T1). Active Flood Plain of Yamuna River is restricted within the present-day bank limits of these rivers and is generally represented by point bars, channel bars, and lateral bars. The environmental hazards of the area include seasonal flooding of terrace zones, seasonal water logging in tals, palaeo-channels and along canals, land degradation due to badland formation along Yamuna and reh infestation or soil alkalization near waterlogged bodies.

5.3. Geostrata and Subsoil Investigation

In general, no one is permitted by the Government of India for drilling boreholes to investigate the geo-strata and subsoil properties of the Taj Mahal premises. Consequently, Authors have decided to the used past published research work, which has provided valuable information about the geo-strata and subsoil properties of the area around Taj Mahal. Subsoil data has been accumulated from published article which were

conducted by [47-52], as well as some literature has been collected from Archaeological Survey of India (ASI). It is important to consider soil data from all these studies to provide a more accurate subsoil profile. Before the early 1980s, there were no historical records of the subsurface conditions at the Taj Mahal. Total number of ten boring have been reported in the north, east, and west sides of the Taj Mahal, and approx. locations of boreholes are shown in Figure 3.

While repairing the riverside walls in 1957, the Archaeological Survey of India (ASI) discovered a well foundation beneath the building. The well spacing was determined to be 3.76 m centre to centre. Timber piles were also exposed near the riverside wall in 1958 [47].

According to [48], each well is made of stone and lime mortar, with wheels with axles and spokes positioned at regular intervals throughout the depth. According to him, the wells were filled with rubble mixed with lime mortar, and the spaces between the wells were filled with solid stone and lime masonry. The findings of the Indian Archaeological Review 1957-58 [47] back this up. This foundation structure distributes load evenly and allows the entire system to be connected as a single unit. The foundation system is depicted graphically in Figure 3.

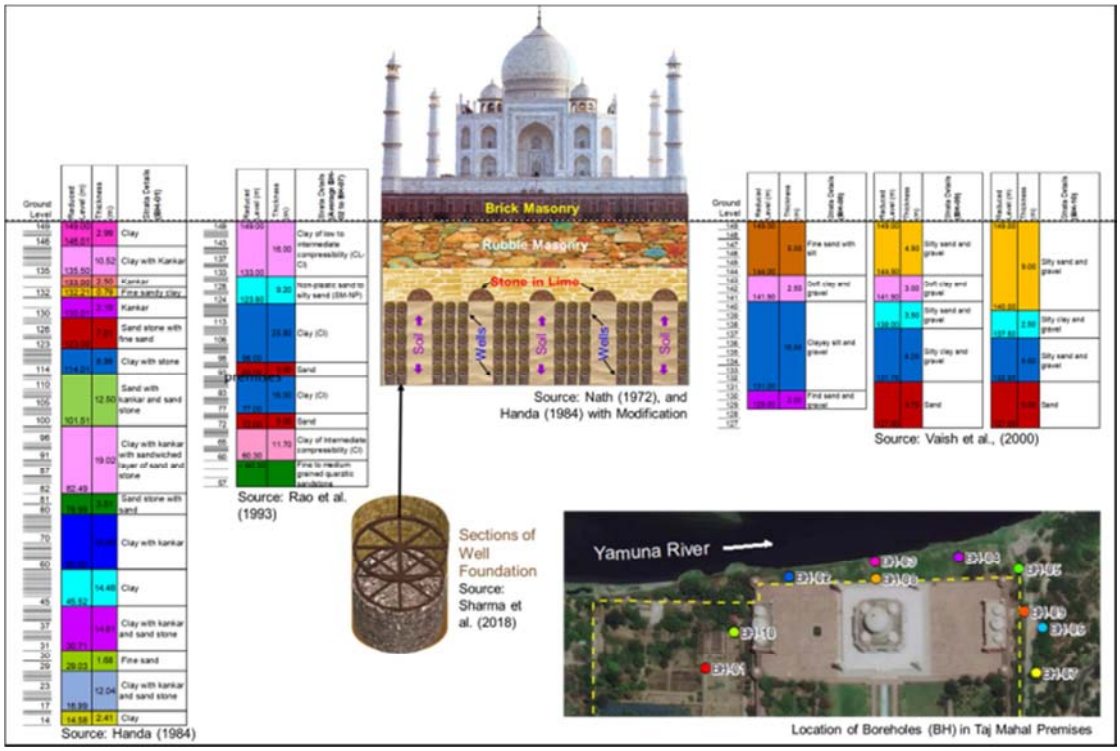

Figure 3. Geo-strata and Sub-soil Properties of Taj Mahal Area.

The soil characteristics at the Taj Mahal's site are described by [49]. The analysis was based on soil data from a previous borehole sunk by local officials in the 1980s to operate the Taj Mahal's fountains. The borehole was bored 135 metres below ground level (BH-01). The area around Taj Mahal having deep alluvial deposits where the depth of rock sometimes can be very large. Below ground level there is a layer of 3 m of clay followed by clay with kankar up to 13.50 m depth. This is underlain by 2.5 m deep kankar layer, followed by 0.8 m deep fine sandy clay, 2.19 m of kankar and 7.01 m deep deposit of sandstone with fine sand. Then there exists 9 m deep clay with stone and 12.5 m deep sand with kankar and sandstone up to a depth of 47.5 m below ground surface. This is followed mostly by deposits of clay with impregnations of kankar and sand at times and with sandwiched layers of sandstone and sand at some depths.

The subsoil stratification of the 350-years old Taj Mahal had been studied by [50]. They have presented soil profiles obtained from six boreholes (BH-02 to BH-07) drilled along the periphery and away from the plinth of the Taj Mahal to depths of about 89 m. Four boreholes (BH-02 to BH-05) have been located between the Taj Mahal and the Yamuna River, whereas boreholes BH-06 and BH-07 lie to the east of the Taj Mahal (Figure 3). The soil samples were examined in the lab to determine the physical and engineering qualities of the area surrounding the Taj Mahal. They created a soil profile based on six boreholes (BH-02 to BH-07) conducted for their research, as well as a deeper borehole (135 m) previously drilled. From reduced level (RL) 149 to 133 m, clay of low-to-intermediate compressibility (CL-CI) was discovered, followed by non-plastic to silty sand (SP-SM) from RL 133 to 123.8 m. From 123.8 to 60.3 m, a thicker clay layer with intermediate compressibility appeared. Below 60.3 m,

fine-to-medium-grained quarzitic sandstone was discovered. The groundwater table was likewise found at 145.2 m (approximately 4 m below ground level), which is consistent with prior findings. Only the layer containing clay soil, according to this study, would show significant consolidation behaviour. [50] determined that since the Taj Mahal's building in 1653, 99.4% of the ultimate settling has occurred.

The ground-penetrating radar (GPR) investigations at three locations in 2000 has been carried-out by [51]. 1st location is situated near the northern boundary of the monument (BH-08), while 2nd (BH-09) and 3rd (BH-10) locations are situated near the marble floor of the mausoleum (Figure 3). To verify the GPR data, three boreholes (BH-08 to BH-10) were dug. The GPR data revealed well foundations at a depth of 17.5 m beneath the structure. In addition, the GPR results were compared to previously collected borehole data (BH-01) and six dug boreholes (BH-02 to BH-07). The groundwater table was also revealed by GPR data at a depth of 5.25 m below the level of GPR profiling. Figure 3 depicts the soil strata of the several boreholes.

The foundation was built on masonry wells that were strengthened with sagwan (teak) wood wheels, as suggested by [52] in his book. These wheels would be spaced out along the vertical length at regular intervals. The wells were filled with riverside soil and rubble. Above the wells would be piers joined by brick arches, on which the structure's red sandstone foundation would rest. Stone and lime mortar would next be used to fill the remaining area.

5.4. River Morphology

5.4.1. Mean River Width

The cross section of a river can be defined as the change of depth (height) of a river with respect to the horizontal distance from one river to the other. The changing form of river cross section is a well-known parameter of a river's health. The average river length (1972-2021) in the study reach starting from 27° 17' 55" N latitude, 77° 49' 57" E longitude, and end at 27° 05' 00" N latitude, 78° 16' 21" E longitude is 114.67 Km. Total 113 cross-sections (at 1 Km interval) have been established on Yamuna River within the study reach. The river width has been measured at each cross-section by using multi-temporal Landsat satellite remote sensing data from 1972 to 2021 (11 in total). Overall mean river width in this reach is 144 m.

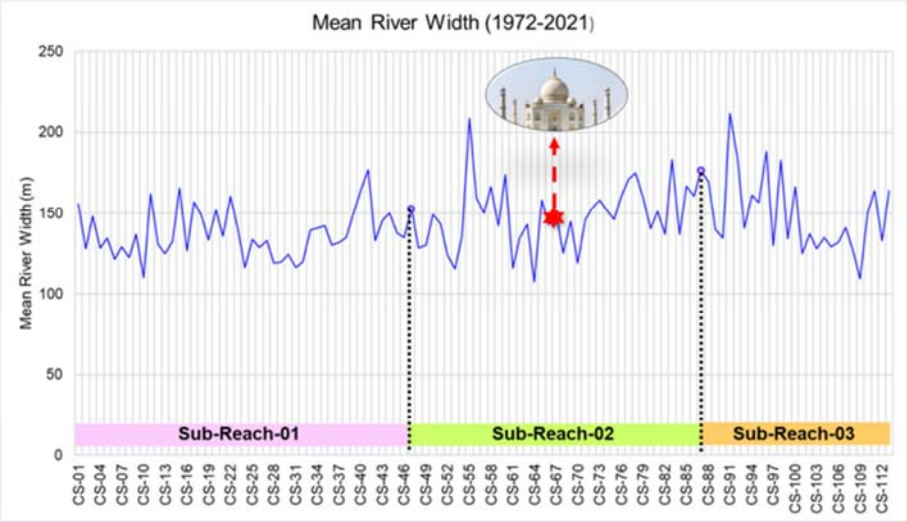

Figure 4. Mean River Width (1972-2021).

Taj Mahal structure is situated at CS-67. For comparative analysis of mean river width, Authors have divided this reach in three sub-reaches i.e. CS-01 to CS-47, CS-48 to CS-86, and CS-87 to CS-113. The mean river width in sub-reach-01 is 137.62 m, in sub-reach-02 is 147.95 m, and in sub-reach-03 is 150.14 m, while the mean river width of CS-67 (where Taj Mahal is situated) is 149.59 m. 113 cross-sections vs river width (m) has been plotted and shown in Figure 4. it is observed that river width is large in the flood year.

5.4.2. Sinuosity Index

Sinuosity is a term used to describe the degree of meandering in a riverbed, which is subsequently used to categorise geomorphological river types [35, 42-45, 65]. Sinuosity is a quantitative index of stream meandering and a distinctive property of channel pattern. Among the variables involved in the geometry and dynamics of alluvial channels, sinuosity is functionally related to morphological, sedimentological, and hydraulic characteristics. Sinuosity has been utilized in functional, comparative, and historical studies. Straight rivers are uncommon in the natural world, and many of them are the product of structural restrictions or sections that connect a succession of meanders. The sinuosity index (Si) has been divided into four alluvial river groups by [66]. According to

them, if Si are "less than 1.05, 1.06-1.25, 1.26-1.50, and 1.51-4.00", then river classes are "straight, sinuous, moderate meandering, and meandering form" respectively.

The length of the talweg (channel length-CL) is divided by the length of the valley (valley length-VL) is well-defined by [66]. CL's and VL's have been measured on multi-temporal Landsat satellite imageries from 1972-2021 (11 in total) by using ArcGIS 10.7.1 software, and sinuosity index (Si) has been calculated, and given in Table 4.

Table 4. Sinuosity Index and Geomorphological River Types.

S. No.	Year	Channel Length (Km)	Valley Length (Km)	Sinuosity Index	River Classes
1	1972	113.37	49.69	2.28	Meandering Form
2	1977	113.42	49.69	2.28	Meandering Form
3	1981	114.29	49.69	2.30	Meandering Form
4	1986	114.56	49.69	2.31	Meandering Form
5	1991	117.69	49.69	2.37	Meandering Form
6	1995	114.60	49.69	2.31	Meandering Form
7	2001	116.80	49.69	2.35	Meandering Form
8	2006	114.65	49.69	2.31	Meandering Form
9	2011	113.81	49.69	2.29	Meandering Form
10	2016	114.68	49.69	2.31	Meandering Form
11	2021	113.54	49.69	2.29	Meandering Form
			Average	2.31	Meandering Form

The gradient of riverbeds is commonly declared to be one of the most strongly weighted explanations when it comes to the origin of sinuosity [65]. The maximum Si has been notices in year 1991 with 2.37, while the minimum Si has been found in year 1972 with 2.28. The average sinuosity index of Yamuna River (within study reach) is 2.31 which corresponding to the highly meandering form of the river. Because of tectonic control is less potent than other variables, the Yamuna River (within study reach) is heavily meandering morphology is governed more by the gradient, lithology, and river environment [35]. As a result, with low gradients, the interaction between the current's energy and the substrate's resistance becomes more dynamic, resulting in cut-offs, river migrations, and other phenomena [33].

5.4.3. Meander Bends Trend Analysis

In a meandering river, migration is caused by erosion on the outer bank and comparable sedimentation on the inner bank [67]. The erodibility of banks is the rule rather than the exception in alluvial river systems [68]. The eroded bank material is moved downstream to the next point bar, where bar deposition and advancement often balance off outer bank erosion. The Taj Mahal has gone through various climatic, environmental, and geotechnical changes in its long history (350-years), and it is located on a meander bend. Therefore, authors have decided to do the meander bends trend of the study area. For meander bend trend analysis total 12 bends have selected in study reach of Yamuna River (Figure 1). Bend No. 01, 03, 05, 07, 09, 10, 12 have situated on left river bankline, while Bend No. 02, 04, 06, 08, 11 have situated on right river bankline, and Taj Mahal has located at bend No. 08, right river bankline. Meander bends migration data has been extracted from 1972 to 2021 by using Landsat satellite imageries of years 1972, 1977, 1981, 1986, 1991, 1995, 2001, 2006, 2011, 2016, and 2021. The meander bends migration data (A) and cumulated meander bends migration data (B) are given in Table 5. A positive value (+) indicates that the meander bend has migrated to right direction from previous study year, while a negative value (-) indicates that the meander bend has migrated to left direction from previous study year.

Table 5. Meander Bends Migration Data (A), and Cumulated Meander Bends Migration Data (B) from 1972-2021.

Years	72-77	77-81	81-86	86-91	91-95	95-01	01-06	06-11	11-16	16-21
	(A) Meander Bends Migration Data									
Bend-01	-23.8	108.3	-338.2	-22.4	6.2	367.8	-278.3	-117.0	14.3	-13.2
Bend-02	9.4	68.2	-6.4	-32.2	7.6	43.1	-77.2	58.8	-20.8	10.4
Bend-03	13.1	58.4	-108.0	60.2	8.6	-15.5	21.2	10.2	-31.0	24.0
Bend-04	8.8	43.4	23.6	8.0	-10.8	-7.5	14.8	-10.8	12.6	-13.4
Bend-05	-43.9	-82.6	94.4	-169.2	-76.8	-221.8	-52.3	-10.4	316.7	-158.3
Bend-06	64.0	1355.5	143.3	83.3	-321.8	343.3	-74.7	83.3	-100.7	112.3
Bend-07	6.1	87.9	-14.3	-68.3	37.3	8.5	64.9	-16.7	82.5	15.6
Bend-08*	37.9	585.7	129.7	-11.9	-16.5	-557.8	-34.1	-50.5	-16.5	47.7
Bend-09	-11.6	34.8	-62.5	-31.7	322.5	-304.6	7.9	15.0	-11.5	22.4
Bend-10	7.6	29.7	871.9	-127.3	-22.0	-53.6	199.0	172.3	-433.3	10.9
Bend-11	-8.8	-11.3	-27.7	-65.5	-5.5	-13.8	34.3	13.8	-111.5	96.2
Bend-12	3.8	12.6	32.0	58.6	15.9	-6.8	-25.4	42.9	-25.4	28.1
	(B) Cumulated Meander Bends Migration Data									
Bend-01	-23.8	84.5	-253.7	-276.1	-269.9	97.9	-180.4	-297.5	-283.2	-296.4

Years	72-77	77-81	81-86	86-91	91-95	95-01	01-06	06-11	11-16	16-21
Bend-02	9.4	77.6	71.1	38.9	46.5	89.6	12.4	71.2	50.4	60.8
Bend-03	13.1	71.5	-36.5	23.7	32.2	16.7	37.9	48.1	17.1	41.1
Bend-04	8.8	52.2	75.8	83.8	73.1	65.5	80.3	69.6	82.1	68.7
Bend-05	-43.9	-126.5	-32.1	-201.2	-278.0	-499.8	-552.1	-562.5	-245.8	-404.2
Bend-06	64.0	1419.4	1562.7	1646.0	1324.3	1667.6	1592.9	1676.1	1575.5	1687.8
Bend-07	6.1	93.9	79.6	11.3	48.6	57.2	122.1	105.4	187.9	203.4
Bend-08*	37.9	623.6	753.2	741.3	724.8	167.0	132.9	82.4	65.9	113.6
Bend-09	-11.6	23.2	-39.3	-70.9	251.6	-53.1	-45.2	-30.2	-41.7	-19.3
Bend-10	7.6	37.3	909.2	781.9	759.9	706.3	905.2	1077.5	644.2	655.2
Bend-11	-8.8	-20.1	-47.8	-113.3	-118.8	-132.6	-98.3	-84.5	-196.0	-99.8
Bend-12	3.8	16.4	48.4	107.0	122.9	116.1	90.6	133.6	108.2	136.2

Through the cumulated meander bends migration data, it is possible to know the trend of any meander bend. The bend migration data from 1972 to 2021 has been analyzed, and trend of all 12 bends have gotten, which is shown in Figure 5.

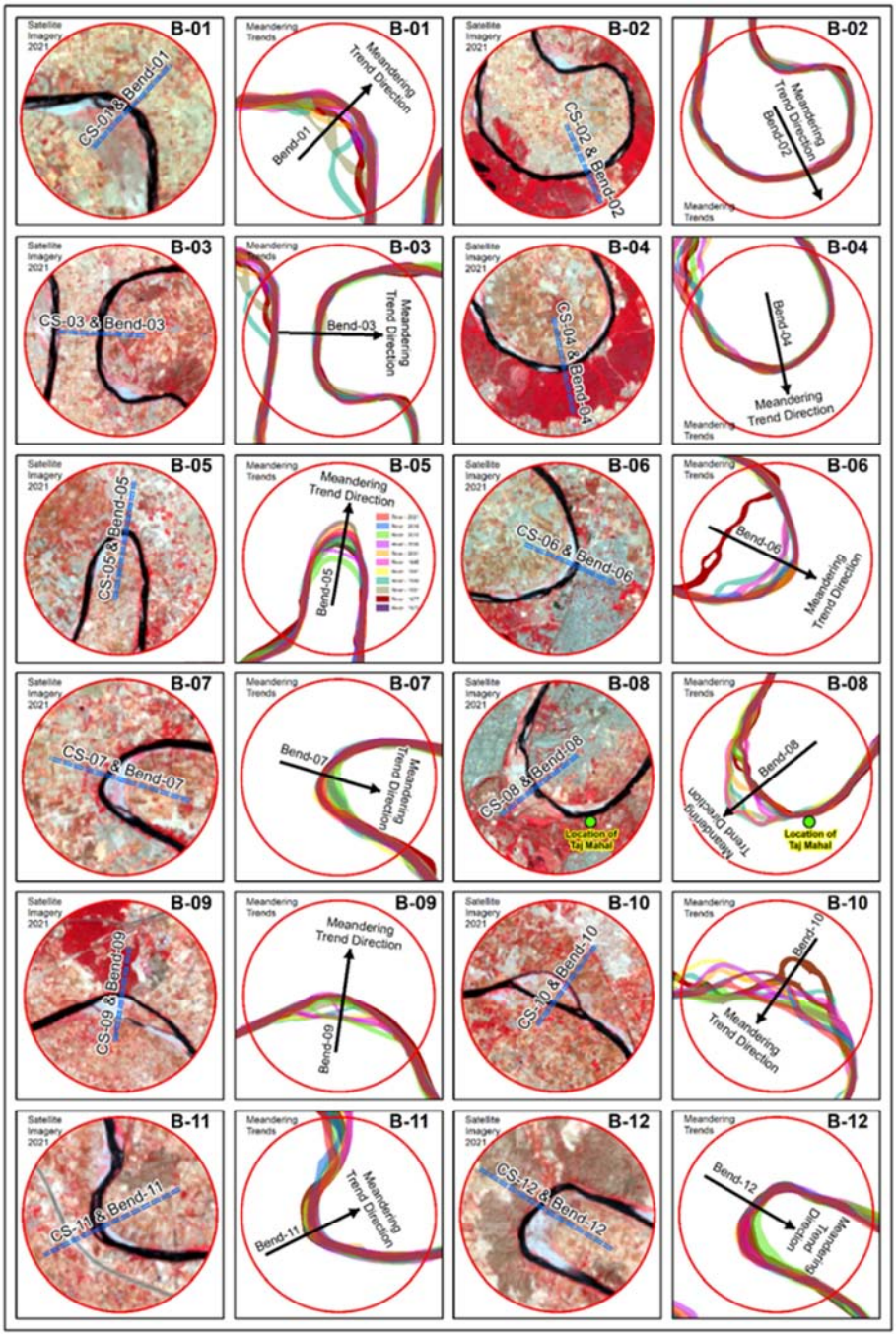

Figure 5. Meander Bends Direction Map.

Referring to the Figure 5, meander bend no. 01, 02, 04, 05, 06, 08, and 09 are continuously migrating towards in meander bend direction, while the meander bend no. 03, 07, 10, 11, and 12 are migrating in opposite direction of meander bends. The migration rate (meter / year) of bend no. 01, 02, 03, 04, 05, 06, 07, 08, 09, 10, 11, and 12 are 5.93 (m/y), 1.22, 0.82, 1.37, 8.08, 33.76, 4.07, 2.27, 0.39, 13.10, 2.00 and 2.72 (m/y) respectively. The maximum migration rate has been observed at bend no. 06, while the minimum has been observed at bend no. 09 (just after the Taj Mahal). The migration rate of bend no. 08 (where the Taj Mahal is situated) is only 2.27 meter/year, because two spurs upstream of the Taj Mahal have been constructed to train the river suitably so as to avoid any threat to the structure of the Taj Mahal and keep the river from attacking the foundations [49]. Over three and a half centuries, the system appears to have operated successfully and survived high floods.

The cross-sectional profile of each cross-section (which is located at the center of meander bends) has been generated by using SRTM DEM data and shown in Figure 6. The all-CS profiles have demonstrated the undulation riverbed surface except the cross-sectional profile of bend no. 8, where the Taj Mahal is situated, here riverbed surface is showing the flat surface throughout the river width. Behind the Taj Mahal, in the Yamuna River some human intervention has observed. A low-level weir up to RL of 146 m across the Yamuna River to impound water to create a permanent lake of water behind the Taj Mahal has been constructed [50]. They have also examined the effect of impounding water on foundation performance and found that these has no influence on the behaviour of subsoil strata and hence on the performance of the foundations of' Taj Mahal as well as no problem to the stability of' Taj Mahal.

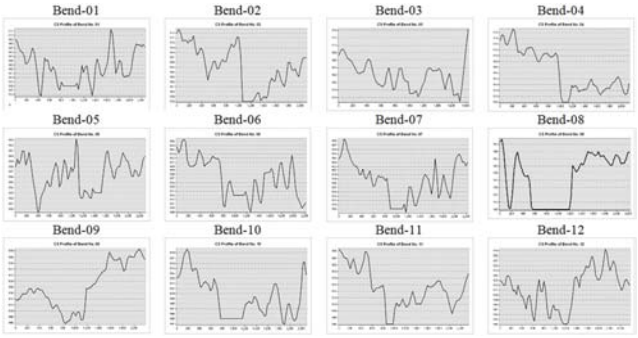

Figure 6. Cross-Sectional Profile of Meander Bends.

5.5. Urban Geomorphology

Local landforms have played an important part in the selection of settlement locations throughout history, and urban geomorphology has affected the evolution of many towns [69]. Urban planning is incomplete without considering the geomorphology and geology of the area [35]. Towns are adjusted to the topography and topography is also adjusted to the needs of construction and planning [70].

Multi-temporal series satellite remote sensing data viz Landsat-1 MSS, Landsat-2 MSS, Landsat-3 MSS, Landsat-5 TM, Landsat-7 ETM+, and Landsat-8 OLI from 1972 to 2021; and vectorization methods were used for extraction of urban expansion of Agra town, it offers a visual and historical overview of the place The data was assembled and integrated using ArcGIS 10.7.1 software to build the spatio-temporal urban map of Agra. Table 6 shows the urban expansion of Agra town as a function of population growth.

Table 6. Urban Expansion corresponding to the Population Growth in Agra City.

S. No.	Years	Population	Population Growth (%)	Urban Area (Km^2)	Urban Expansion Growth (%)
1	1971	591,917	28.12	11.21$^{\#}$	
2	1977*	648,000	09.47	15.72	40.16
3	1981	694,191	07.13	18.97	20.67
4	1986*	855,000	23.16	30.70	61.85
5	1991	891,790	04.30	50.30	63.85
6	1995*	1,123,000	25.93	66.57	32.35
7	2001	1,275,134	13.55	79.55	19.50
8	2006*	1,568,000	22.97	84.23	5.88
9	2011	1,585,704	01.13	106.78	26.77
10	2016*	2,009,000	26.69	125.74	17.76
11	2021*	2,262,000	12.59	155.21	23.44

* Projected Population. United Nations - World Population Prospects. https://www.macrotrends.net/cities/21151/agra/population
# Urban Area of Year - 1972

It has observed from multi-temporal, multi-resolution and multi-spectral satellite data interpretation from 1972 to 2021, that Agra city has experienced a significant urban growth in the last 50 years. Agra urban area has increased 1284% and 13.84 times in the last 5 decades, while the Agra city population has also increased 282% and 3.82 times in the last 5 decade. The urban area of Agra city was respectively 11.21 Km^2 in 1972, 15.72 Km^2 in 1977, 18.97 Km^2 in 1981, 30.70 Km^2 in 1986, 50.30 Km^2 in 1991, 66.57 Km^2 in 1995, 79.55 Km^2 in 2001, 84.23 Km^2 in 2006, 106.78 Km^2 in 2011, 125.74

Km^2 in 2016, and 155.21 Km^2 in 2021 (Table 6). The Agra city has extended by 144 Km^2 in the period of 1972-2021 with an average growth rate of 2.88 Km^2 per year.

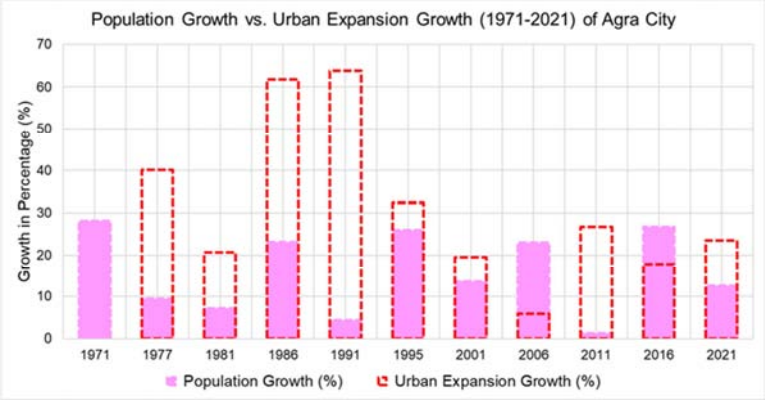

Figure 7. Population Growth vs. Urban Expansion Growth (1971-2021) of Agra City.

In the last 5 decades, it has observed that the maximum population growth found in the period of 1961-1971 with 28.12%, then 2011-2016 with 26.69%, while the minimum population growth found in the period of 2006-2011 with 01.13%, then 1986-1991 with 04.30%. It has also observed that the maximum urban expansion growth found in the period of 1986-1991 with 63.85%, then 1981-1986 with 61.85%, while the minimum urban expansion growth found in the period of 2001-2006 with 5.88%, then 2011-2016 with 17.76% (Figure 7). It is also seen that there has been a lot of urban expansion in 1991 and 2011, but population growth has decreased in comparison, but we have seen the opposite combination in 2006 and 2016.

Authors have analyzed the urban expansion data by keeping the Taj Mahal in the center. The urban expansion is divided in 32 directions, which is given in Table 7.

Table 7. Urban Expansion Data with the Taj Mahal as the Centerpiece (1972-2021).

Direction	1972	1977	1981	1986	1991	1995	2001	2006	2011	2016	2021
N	0.13	0.53	0.62	1.43	2.62	3.17	4.25	4.52	5.70	6.49	8.29
NbyE	0.52	0.53	0.53	0.77	1.22	1.81	2.38	2.53	3.33	4.39	5.47
NNE	0.02	0.02	0.02	0.58	1.26	1.74	1.84	2.25	2.32	2.37	2.81
NEbyN	-	-	-	-	0.02	0.49	0.62	0.67	0.73	0.99	1.09
NE	-	-	-	-	-	-	0.15	0.38	0.58	0.97	1.20
NEbE	-	-	-	-	-	-	-	-	-	-	-
ENE	-	-	-	-	-	0.00	0.00	0.00	0.00	0.00	0.00
EbyN	-	-	-	0.00	0.00	0.03	0.03	0.03	0.09	0.15	0.29
E	-	0.01	0.01	0.04	0.04	0.09	0.16	0.16	0.46	0.47	0.57
EbyS	-	0.04	0.04	0.08	0.11	0.20	0.34	0.34	0.41	0.41	0.93
ESE	0.03	0.08	0.08	0.16	0.20	0.36	0.60	0.60	0.92	1.13	1.56
SEbE	0.08	0.16	0.20	0.22	0.27	0.30	0.48	0.48	0.72	2.10	2.67
SE	0.08	0.14	0.24	0.30	0.30	0.30	0.35	0.38	0.59	1.66	1.66
SEbyS	0.06	0.09	0.12	0.29	0.31	0.31	0.37	0.42	0.82	1.25	1.31
SSE	0.05	0.07	0.07	0.24	0.42	0.55	0.62	0.71	2.22	2.78	3.07
SbyE	0.05	0.07	0.07	0.17	0.47	0.96	1.02	1.16	1.54	2.69	3.30
S	0.04	0.07	0.07	0.10	0.66	0.91	1.05	1.19	1.78	2.33	3.13
SbyW	0.00	0.05	0.04	0.07	0.51	0.82	0.84	0.89	1.99	3.14	3.67
SSW	-	0.02	0.01	0.04	0.23	0.79	1.47	1.76	4.11	4.50	5.58
SWbS	-	0.00	0.01	0.01	0.89	1.02	2.14	2.36	2.72	3.51	4.82
SW	-	-	-	0.02	1.41	1.82	2.14	2.34	3.73	4.42	4.80
SWbW	-	-	-	0.43	1.97	3.06	3.68	3.68	4.10	4.71	6.07
WSW	0.32	0.39	0.39	1.44	3.78	4.11	4.45	4.45	4.56	4.67	5.27
WbyS	1.11	1.61	1.61	2.46	3.23	3.23	3.23	3.23	3.24	3.31	6.36
W	1.32	2.06	2.33	2.98	3.80	4.08	5.26	5.48	7.50	8.90	13.90
WbyN	0.99	1.17	1.75	3.22	4.89	6.28	7.00	7.28	11.31	14.02	15.02
WNW	2.50	2.75	2.98	3.46	4.74	8.55	12.05	13.08	15.52	16.10	16.61
NWbW	1.15	1.66	1.66	3.20	4.50	5.63	6.44	6.73	7.70	8.78	9.38
NW	0.96	1.45	1.86	3.07	4.03	4.78	4.78	4.88	5.19	5.19	5.40
NWbN	1.16	1.54	2.30	2.90	4.21	5.38	5.68	5.87	5.99	6.29	6.93
NNW	0.46	0.67	1.34	1.91	2.85	4.06	4.20	4.30	4.50	5.09	9.29
NbyW	0.15	0.53	0.61	1.08	1.36	1.74	1.94	2.05	2.42	2.92	4.74
Total	11.21	15.72	18.97	30.70	50.30	66.57	79.55	84.23	106.78	125.74	155.21

Referring to Table 7, about 52.36% of urban area has extended in north to west direction, 25.58% of urban area has extended in west to south direction, 12.34% of urban area has extended in north to east direction, and only 9.71% of urban area has extended in east to south direction. Out-of-total urban expansion, around 78% of area has extended in north-west-south direction, while only 22% of area has extended in north-east-south direction (Figure 8). We have seen very good transportation network in the North-West-South direction, which is directly connected to national capital Delhi. While unstable river, gullied tract, and river rugged has noticed in north-east to south-east direction, where only 3.88% of urban area has extended. It has also noticed that the maximum urban area has extended in WNW direction with 10.75%, while the minimum urban area has extended in NEbyE direction with 0.00%.

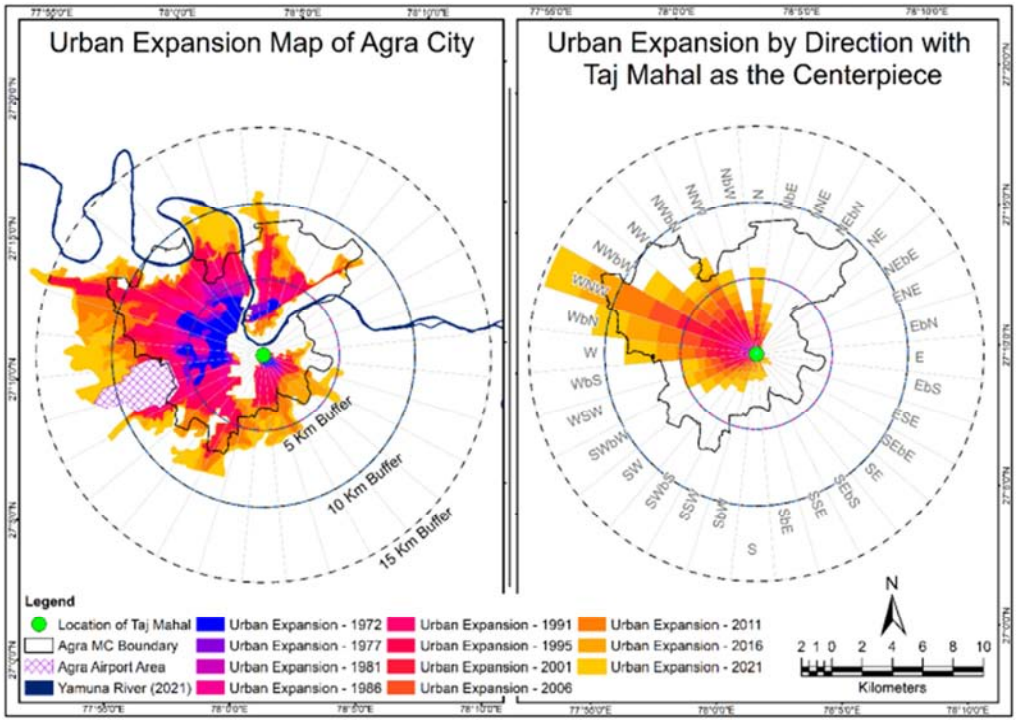

Figure 8. Urban Expansion Map of Agra City.

When urban expansion boundary has overlayed on the geomorphology map, it has notices that till 2001, urban area is limited to only older alluvial plain, but due to alarming increment of population, urban area is extended (2006-2021) to other geomorphic units i.e. older flood plain, gullied tract, active flood plain, channel bar, lateral bar, point bar which are not good for the residence purpose. However, with the development of civilization along the riverbank in modern times, the river changed its course and its point of maximum scour also shifted [36].

The changes in the land use pattern in Agra city due to urbanization has resulted in the frequent of waterlogging and floods. The loss in interconnectivity and marshland has resulted mainly due to the unsystematic growth in the northwestern direction. As the development increased, all the green cover has been reduced to non-vegetative surfaces which resulted in the low infiltration capacity and high surface run-off [36]. In the agricultural areas of the area, the waterlogging condition occurs due to the steady rise in the groundwater table due to inadequate drainage capacity of the area [35].

6. Conclusion

Advances in remote sensing approaches have consistently improved geomorphology by improving mapping technology, form analysis, and feature discrimination. Space-borne and airborne technology now not another innovation, it has been generally utilized since longer than a century. It has been extensively used in geomorphology since 1972, when Landsat series data (from 1972 to present) are freely available, and because the amount to which it can suit geomorphologists' exploratory needs determines its worth. Subsequently, space-borne remotely sensed imageries of L-band Advanced Land Observing Satellite (ALOS) / Phased Array Type L-band Synthetic Aperture Radar (PALSAR), Sentinel-1, Landsat-8 Operational Land Imager (OLI), C-band Shuttle Radar Topography Mission (SRTM) were used in a complementary manner to assess the geological structures, geomorphological investigation and mapping of the study area, while Landsat-1,

2 & 3 MSS, Landsat-5 TM, Landsat-7 ETM+, and Landsat-8 OLI have been used for river morphology (mean river width, sinuosity index, and meander bends trend analysis) and urban expansion / urban geomorphology analysis.

An area of 25 Km buffer from the center of Taj Mahal has been selected for geology, geomorphology, urban geomorphology, and subsoil investigation, while 114 Km long river reach of the Yamuna River (which is fall within the buffer area) is also selected for river morphology study. Geomorphologically, the area has been classified into two broad geomorphic units. (i) upland or older alluvial plain termed as Varanasi older alluvial plain (VOAP), (ii) low land or flood plain comprising older flood plain, which has future classified as erosional terrace (Te) and depositional terrace (T1, T1a), and active flood plain of present-day rivers. Geo-strata and sub-soil data have been accumulated from past studies, which has provided valuable information about the geo-strata and subsoil properties of the area around Taj Mahal. According to them, (i) clay of low-to-intermediate compressibility, (ii) non-plastic to silty-sand, (iiI) thicker clay layer of intermediate compressibility was found from RL 149-133 m, 133-123.8 m, 123.8-60.3 m respectively, while fine-to-medium-grained quarzitic sandstone was found below 60.3 m.

Overall mean river width of the study reach is 144 m, while the mean river width just behind the Taj Mahal is 149.6 m. The average sinuosity index of the study reach is 2.31 which corresponding to the highly meandering form of the river. It is because tectonic control is less powerful than other variables, the meandering is more influenced by the gradient, lithology and river surrounding. Total twelve meander bends have been analyzed, and the minimum bend migration rate has been observed at bend no. 09 d/s of Taj Mahal, while the bend migration rate of bend no. 08 (where the Taj Mahal is situated) is only 2.27 meter/year, because two spurs u/s of the Taj Mahal have been installed to train the river and to avoid any threat to the structure of the Taj Mahal. Through the cross-sectional profile analysis, some human intervention has observed behind the Taj Mahal, and notices that a low-level weir up to a RL of 146 m has been constructed across the Yamuna River to create a permanent lake of water behind the Taj Mahal. Agra city has experienced a significant urban growth in the last 50 years (1972-2021). In the last 5 decades, it has increased 1284% of urban area with an average growth rate of 2.88 Km^2 per year, while population has increased only 282%. Till 2001 urban area is limited to only one geomorphic unit of older alluvial plain, but onwards due to indiscriminate of population increment it has been extended to other geomorphic units, which is not good for the residence purpose.

Acknowledgements

Authors are grateful to Managing Director, DHI (India) Water and Environment Pvt Ltd, New Delhi, India for providing the necessary facilities to carry out this work.

References

[1] Verstappen HTh. 1977. Remote sensing in geomorphology. Elsevier's Amsterdam.

[2] Rosenfeld CL. 1984. Remote sensing techniques for geomorphologists. In: Costa JE, Fleisher PJ. (Eds) Developments and Applications of Geomorphology. Springer, Berlin, Heidelberg.

[3] Abdelkareem M, Kamal El-Din G and Osman I. 2018. An integrated approach for mapping mineral resources in the eastern desert of Egypt. International Journal of Applied Earth Observation and Geoinformation. Vol. 73C, pp. 682-696.

[4] Lee WT. 1922. The face of the earth as seen from the air. Special Publication 4, American Geographical Society, New York.

[5] Lobeck AK. 1933. Airways of America, Guidebook, No. 1, The United Air Lines. A geological and geographical description of the route from New York to Chicago and San Francisco. NY Geographic Press, Columbia University.

[6] Fenneman NM. 1931. Physiography of the western United States. McGraw-Hill Book Company, NY.

[7] Fenneman NM. 1938. Physiography of the eastern United States. McGraw-Hill Book Company, NY.

[8] Troll C. 1939. Aerial plan and ecological soil research. Zeits F Gessell. Erdk. Berlin. Vol. 7/8, pp. 241-298.

[9] Bobeck H. 1941. Aerial view and geomorphology. Hansa Aerial Photo, Berlin.

[10] Belcher D. 1946. Engineering applications of aerial reconnaissance. Geological Society of America Bulletin. Vol. 678), pp. 727-734.

[11] Frost RE. 1952. Discussion of photo recognition, analysis, and interpretation. Photogrammetric Engineering. Vol. 18, pp. 502-505.

[12] Gandillot J. 1954. Aerial photography at the service of geology. Bulletin of the Geological Society of France. Vol. 6 (4), pp. 45-50.

[13] Stone KH. 1951. Geographical air-photo interpretation. Photogrammetric Engineering. Vol. 17, pp. 754-759.

[14] Lattman LH. 1963. Geologic interpretation of airborne infrared imagery. Photogrammetric Engineering. Vol. 29, pp. 83-87.

[15] MacDonald HC. 1969. Geologic evaluation of radar imagery from Darien Province, Panama. Modern Geology. Vol. I, pp. 1-64.

[16] Keuttner J. 1968. Man's geophysical environment: its study from space. U.S. Department of Commerce, Environmental Science Services Administration, Washington.

[17] Smith MJ and Pain C. 2009. Applications of remote sensing in geomorphology. Progress in Physical Geography. Vol. 33, pp. 568-582.

[18] Thurmond AK, Stern RJ, Abdelsalam MG, Nielsen KC, Abdeen MM and Hinz E. 2004. The Nubian swells. Journal of African Earth Sciences. Vol. 39, pp. 401-407.

[19] Paillou P, Schuster M, Tooth S, Farr T, Rosenqvist A and Lopez S. 2009. Mapping of a major paleo-drainage system in eastern Libya using orbital imaging radar: the Kufra River. Earth and Planetary Science Letters. Vol. 277 (3-4), pp. 327-333.

[20] Breeze PS, Drake NA, Groucutt HS, Parton A, Jennings RP, White TS, Clark-Balzan L, Shipton C, Scerri EML, Stimpson CM, Crassard R, Hilbert Y, Alsharekh A, Al-Omari A and Petraglia MD. 2015. Remote sensing and GIS techniques for reconstructing Arabian palaeohydrology and identifying archaeological sites. Quaternary International. Vol. 382, pp. 98-119.

[21] Roth LE and Elachi C. 1975. Coherent electromagnetic losses by scattering from volume inhomogeneities, IEEE Transactions on Antennas and Propagation. Vol. 23, pp. 674-675.

[22] Gaber A, Abdelkareem M, Abdelsadek I, Koch M and El-Baz F. 2018. Using InSAR coherence for investigating the interplay of fluvial and aeolian features in arid lands: implications for groundwater potential in Egypt. Remote Sensing. Vol. 10 (6), pp. 832-849.

[23] Lee H. 2001. Interferometric synthetic aperture radar coherence imagery for land surface change detection. University of London.

[24] Jung J, Kim D. 2016. Coherent change detection using InSAR temporal decorrelation model: a case study for volcanic ash detection. IEEE Transactions on Geoscience and Remote Sensing. Vol. 54 (10), pp. 5765-5775.

[25] Havivi S, Amirb D, Schvartzman I, August Y, Maman S, Rotman S and Blumberg D. 2018. Mapping dune dynamics by InSAR coherence. Earth Surface Processes and Landforms. Vol. 43, pp. 1229-1240.

[26] Abdalla F, Moubark K and Abdelkareem M. 2016. Impacts of human activities on destruction of the archeological sites in southern Egypt using remote sensing and field data. Journal of Environmental Science and Management. Vol. 19 (2), pp. 15-26.

[27] Huang C, Chen Y, Zhang S and Wu J. 2018. Detecting, extracting, and monitoring surface water from space using optical sensors: a review. Reviews of Geophysics. Vol. 56, pp. 333-360.

[28] Pareta K. 2003. Morphometric analysis of Dhasan river basin, India. Uttar Bharat Bhoogol Patrika, Gorakhpur. Vol. 39, pp. 15-35.

[29] Pareta K. 2004. Hydro-geomorphology of Sagar district (M. P.): a study through remote sensing technique. In: 19th M. P. Young Scientist Congress, Madhya Pradesh Council of Science & Technology (MAPCOST) Bhopal.

[30] Pareta K. 2004. Geomorphological and hydro-geological study of Dhasan river basin, India using remote sensing techniques. Unpublished Ph. D. Thesis, Dr Hari Singh Gour University, Sagar M. P.

[31] Pareta K. 2011. Geo-environmental and geo-hydrological study of Rajghat dam, Sagar MP using remote sensing techniques. International Journal of Scientific & Engineering Research. Vol. 2 (8), pp. 1-8.

[32] Pareta K and Pareta U. 2011. Hydromorphogeological study of Karawan watershed using GIS and remote sensing techniques. International Scientific Research Journal. Vol. 3 (4), pp. 243-268.

[33] Pareta K and Pareta U. 2011. Quantitative morphometric analysis of a watershed of Yamuna basin, India using ASTER (DEM) data and GIS. International Journal of Geomatics and Geosciences. Vol. 2 (1), pp. 248-269.

[34] Pareta K and Pareta U. 2012. Quantitative geomorphological analysis of a watershed of Ravi River basin, H. P. India. International Journal of Remote Sensing & GIS. Vol. 1 (1), pp. 47-62.

[35] Pareta K and Pareta U. 2012. Quantitative morphometric analysis of a watershed: based on digital terrain model and GIS. LAP Lambert Academic Publishing, Germany. pp. 1-93.

[36] Pareta K. 2012. Geomorphic control on urban expansion - a case study of Sagar town MP. International Journal of Advanced Scientific and Technical Research. Vol. 1 (2), pp. 20-29.

[37] Pareta K. 2013. Geomorphology and hydrogeology: applications and techniques using remote sensing and GIS. LAP Lambert Academic Publishing, Germany. pp. 1-413.

[38] Pareta K and Pareta U. 2013. Geological investigation of Rahatgarh waterfall of Sagar (M. P.) through the field survey and satellite remote sensing techniques. International Journal of Geology. Vol. 5 (3), pp. 72-79.

[39] Pareta K and Pareta U. 2015. Geomorphological interpretation through satellite imagery & DEM data. American Journal of Geophysics, Geochemistry and Geo-systems. Vol. 1 (2), pp. 19-36.

[40] Pareta K and Pareta U. 2016. Landform classification and geomorphological mapping of Ramgarh structure, Rajasthan (India) through remote sensing and geographic information system (GIS). Journal of Hydrology and Environment Research. Vol. 4 (1), pp. 1-17.

[41] Pareta K and Pareta U. 2017. Geomorphological analysis and hydrological potential zone of Baira river watershed, Churah in Chamba district of Himachal Pradesh, India. Indonesian Journal of Science and Technology. Vol. 2 (1), pp. 26-49.

[42] Pareta K, Jakobsen F and Joshi M. 2019. Morphological characteristics and vulnerability assessment of Alaknanda, Bhagirathi, Mandakini and Kali rivers, Uttarakhand (India). American Journal of Geophysics, Geochemistry and Geosystems. Vol. 5 (2), pp. 49-68.

[43] Pareta K and Pareta U. 2019. Geomorphic classification and mapping of Rapti river system using satellite remote sensing data. American Journal of Geophysics, Geochemistry and Geosystems, Vol. 6 (1), pp. 1-15.

[44] Pareta K and Pareta U. 2019. Hydro-geomorphological mapping of Rapti river basin (India) using ALOS PALSAR (DEM) data, GRACE / GLDAS data, and Landsat-8 satellite remote sensing data. American Journal of Geophysics, Geochemistry and Geosystems. Vol. 5 (3), pp. 91-103.

[45] Pareta K. 2021. Historical morpho-dynamics and hydromorphogeobathymetry investigation of an area around Dibru-Saikhowa national park, Assam. American Journal of Geophysics, Geochemistry and Geosystems. Vol. 7 (2), pp. 85-100.

[46] NGRI. 1993. Geophysical investigations related to the preservation and assessing the stability of Taj Mahal. Technical Report NGRI 93-Exp-139, NGRI Hyderabad (India).

[47] Ghosh A. 1958. Indian Archaeology 1957-58: A Review. Department of Archaeology, Government of India, New Delhi, India.

[48] Nath R. 1972. The immortal Taj Mahal: the evolution of the tomb in Mughal Architecture. D. B. Taraporevala Sons, Bombay, India.

[49] Handa SC. 1984. Foundation performance of very old Structures. International Conference on Case Histories in Geotechnical Engineering, Arlington, Virginia, USA, 6 May, Paper 23.

[50] Rao ASR, Saran S, Handa SC, Ramasamy G and Viladkar MN. 1993. Taj Mahal - an appraisal of foundation performance. International Conference on Case Histories in Geotechnical Engineering, 1 June, St Louis, MO, USA, Paper 57.

[51] Vaish JN and Sharma RS. 2000. Ground-probing radar investigations for foundation and other subsurface features at a historical site. 8th International Conference on Ground Penetrating Radar 4084.

[52] Nath R and Nath A. 2010. Taj Mahal, history and architecture. Historical Research Documentation Programme, Jaipur, India.

[53] Heron AM. 1911. Geological quadrangle map of Mathura quadrangle. Geological Survey of India.

[54] Das AR. 1972. Geological quadrangle map based on Survey of India map no 54-E. Geological Survey of India.

[55] Singh MHJ. 1973. Geological quadrangle map based on Survey of India map no 54-E. Geological Survey of India.

[56] Dutta AK and Singh SP. 1973. Geological quadrangle map of Mathura quadrangle, Haryana-Rajasthan-Uttar Pradesh. Geological Survey of India.

[57] Sinha KK. 1973. Geological quadrangle map, Agra quadrangle Uttar Pradesh. Geological Survey of India.

[58] Sinha PN. 1974. Geological quadrangle map of Mathura quadrangle, Haryana-Rajasthan-Uttar Pradesh. Geological Survey of India.

[59] Khan AU and Nigam AC. 1985. Geological quadrangle map of Agra. Geological Survey of India.

[60] Singh OR and Nambiar KV. 1987. Geological quadrangle map of Agra. Geological Survey of India.

[61] Dasgupta G and Mujtaba SAI. 1991. Geological quadrangle map based on Survey of India map no 54-I. Geological Survey of India.

[62] Jain VK and Singh H. 1992. Geological quadrangle map, Agra quadrangle Uttar Pradesh. Geological Survey of India.

[63] Singh H and Gupta AK. 1992. Geological quadrangle map based on Survey of India map no 54-I. Geological Survey of India.

[64] Mathur KN, Singh PN, Srivastava VK, Bisaria BK, Kumar R, Khan NA, Upadhyay TP, Shukla RC, Prasad S and Yadav PK. 2002. Quadrangle geological maps and reports. Geological Survey of India, Northern Region, Lucknow.

[65] Horacio J. 2014. River sinuosity index: geomorphological characterization. Technical note 2. CIREF and Wetlands International. pp. 2-7.

[66] Leopold LB and Wolman MG. 1957. River channel patterns; braided, meandering, and straight. U.S. Geological Survey Professional Paper, 282-B.

[67] Julien PY, Klaassen GJ, Ten Brinke WBM and Wilbers AWE. 2002. Case study - bed resistance of Rhines River during 1998 flood. Journal of Hydraulic Engineering. Vol. 128 (12), pp. 1042-1050.

[68] Richardson WR and Thorne CR. 2001. Multiple thread flow and channel bifurcation in a braided river: Brahmaputra-Jamuna River, Bangladesh. Geomorphology. Vol. 38 (3), pp. 185-196.

[69] Bathrellos G. 2007. An overview in urban geology and urban geomorphology. Bulletin of Geological Society of Greece. Vol. 40, pp. 1354-1364.

[70] Ahnert F. 1996. Introduction to geomorphology. London, Arnold.